Motion of Spin-Labeled Side Chains in T4 Lysozyme: Effect of Side Chain Structure†

Hassane S. Mchaourab,‡,§ Tamás Kálai,|| Kálmán Hideg,|| and Wayne L. Hubbell*,‡

Jules Stein Eye Institute and Department Chemistry and Biochemistry, University of California, Los Angeles, California 90095-7008, and Institute of Organic and Medicinal Chemistry, University of Pécs, P.O. Box 99, Pécs H-7643, Hungary

Received November 5, 1998; Revised Manuscript Received December 22, 1998

ABSTRACT: Previous studies have shown that the mobility of nitroxide side chains in a protein, inferred from the electron paramagnetic resonance (EPR) spectra, can be used to classify particular sites as helix surface sites, tertiary contact sites, buried sites, or loop sites. In addition, the sequence dependence of mobility can identify regular secondary structure. However, in the most widely used side chain, an apparent interaction of the nitroxide ring with the protein at some helix surface sites gives rise to EPR spectra degenerate with those at tertiary contact sites. In the present study, we use selected sites in T4 lysozyme to evaluate novel nitroxide side chains designed to resolve this degeneracy. The results indicate that the reagent 3-(methanesulfonylthiomethyl)-2,2,5,5-tetramethylpyrrolidin-1-yloxy reacts with cysteine to give a nitroxide side chain that has a high contrast in mobility between helix surface and tertiary contact sites, effectively resolving the degeneracy. The reagent 3-(iodomercuriomethyl)-2,2,5,5-tetramethyl-2,5-dihydro-1*H*-pyrrol-1-yloxy reacts with cysteine to provide a mercury-linked nitroxide that also shows reduced interaction with the protein at most helix surface sites. Thus, these new side chains may be the preferred choices for structure determination using site-directed spin labeling.

Site-directed spin labeling (SDSL)[1] is emerging as a new tool for determination of structure and conformational dynamics of both water-soluble and membrane proteins of arbitrary molecular weight (for reviews, see refs 1−3). The basic strategy of SDSL is to introduce a paramagnetic nitroxide side chain at a specific site in a protein sequence and to analyze the EPR spectrum of the spin-labeled protein in terms of a set of environmental parameters that characterize the site in the protein fold.

The most useful parameters to date have proven to be side chain solvent accessibility and side chain dynamics. The solvent accessibility is proportional to the Heisenberg exchange frequency of the nitroxide side chain with paramagnetic reagents in solution, a quantity that can be determined experimentally (*2*, *4*). A quantitative description of the dynamic modes of the nitroxide side chain requires simulation of the EPR spectra (*5*), preferably at multiple frequencies, and this remains a goal for future development in SDSL. At a qualitative level, the term "mobility" is employed to grossly characterize the motion of the nitroxide side chain as inferred from general features of the EPR spectrum, such as the width of the $m_I = 0$ resonance line and the spectral second moment (*6*). These measures do not discriminate among different populations in multicomponent spectra, although the line width measure more heavily weighs the mobile component and the second moment measure more heavily weighs the immobile component.

Nitroxide scanning through a region provides a set of environmental parameters that identify sequence-correlated secondary structure, and both α-helical and β-sheet proteins of known structure have been analyzed (*2*−*4*, *6*). In a detailed study of T4L, interhelical loop sites, helix surface sites, tertiary contact sites, and buried sites were partially resolved on the basis of nitroxide side chain mobility alone. For solvent-exposed helix surface sites, it appears possible to further distinguish interior sites (those away from the ends of the helix), N-terminal sites, and C-terminal sites (*6*).

Nitroxide side chain accessibility and mobility provide local structural information. Global information can be obtained from the introduction of two paramagnetic sites and determination of the interspin distance through magnetic spin−spin interactions (*7*−*12*). The combination of local and global information from SDSL can provide sufficient constraints to model the structure of a protein at the level of the backbone fold.

The above SDSL methods have been used to determine the structure in bacteriorhodopsin (*4*, *13*−*15*), rhodopsin (*16*−*21*), colicin E1 (*22*), membrane-bound diphtheria toxin (*23*, *24*), α-crystallin and small heat shock proteins (*25*, *26*), ferric enterobactin receptor (*27*, *28*), lactose permease (*29*, *30*), annexin XII (*31*), T4L (*6*, *7*), and the *Streptomyces lividans* K^+ channel (*3*, *32*).

An important feature of the SDSL approach is that changes in side chain mobility and interspin distance can be measured

† Research reported here was supported by NIH Grants EY05216 (W.L.H.) and EY12018 (H.S.M.), Research to Prevent Blindness (W.L.H.), Jules Stein Professorship Endowment (W.L.H.), and the Hungarian Academy of Sciences, AKP 97-13 2,4/23 (K.H.).

* To whom correspondence should be addressed.

‡ University of California, Los Angeles.

§ Present address: Biophysics Research Institute, Medical College of Wisconsin, Milwaukee, Wisconsin 53226.

|| University of Pécs.

[1] Abbreviations: EPR, electron paramagnetic resonance; SDSL, site-directed spin labeling; T4L, T4 lysozyme; TLC, thin-layer chromatography.

10.1021/bi9826310 CCC: $18.00
Published on Web 02/17/1999

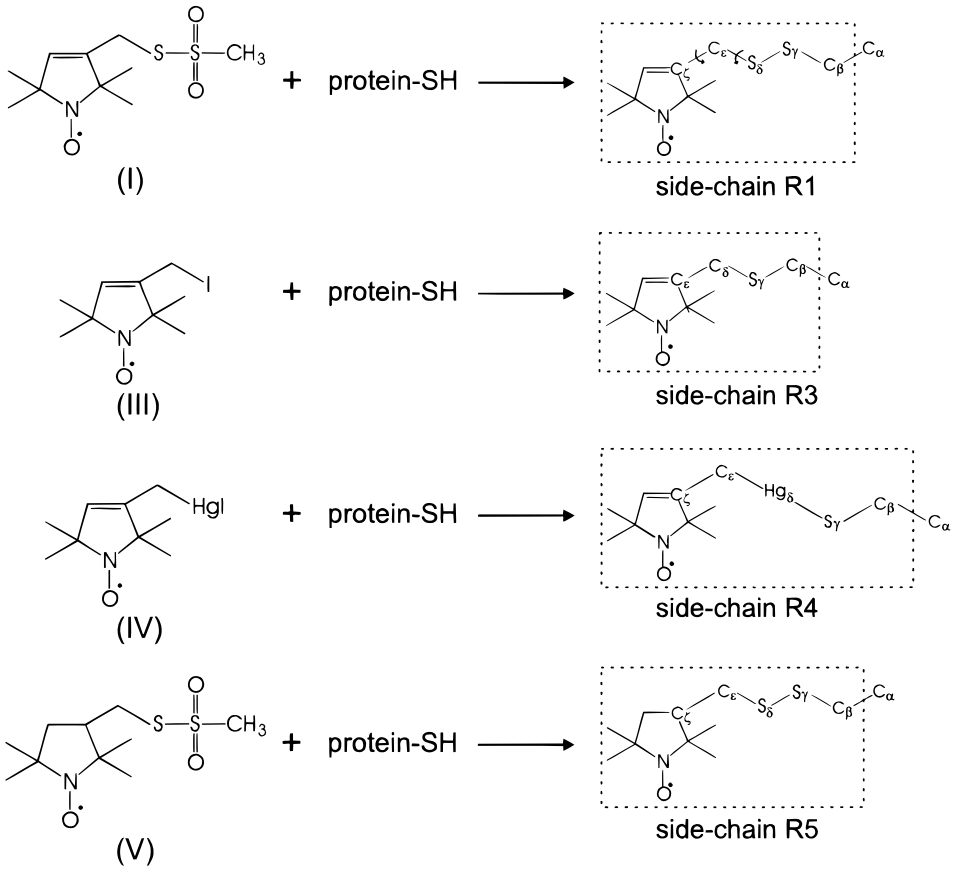

FIGURE 1: Reactions of the spin-labeled reagents **I**, **III**, **IV**, and **V** to generate the corresponding side chains designated R1, R3, R4, and R5. The curved arrows in R1 indicate bonds with the greatest freedom of rotation (see text).

in real time in the millisecond domain with conventional EPR spectrometers. At the present time, SDSL has been employed to time-resolve specific conformational changes associated with photoexcitation of rhodopsin (*33*) and bacteriorhodopsin (*34*−*36*), with membrane binding in colicin E1 (*37*), and upon folding of T4L (*2*) and cytochrome *c* (*38*).

To date, most SDSL studies have employed the disulfide-linked nitroxide side chain designated R1, generated by the reaction of cysteine with the methanethiosulfonate spin label **I** (Figure 1). An analysis of spin-labeled T4L in solution showed that the spectra of R1 at most of the helix surface sites investigated corresponded to a single population of spins undergoing anisotropic motion. Moreover, the mobility of R1 at these sites was found to be essentially independent of the molar volume of the nearest-neighbor side chains at $i\pm3$, $i\pm4$. To account for these results and others, the motion of the R1 side chain at helix surface sites was suggested to be constrained by interaction of the disulfide bond with main chain atoms, effectively immobilizing the $C_\alpha-C_\beta-S_\gamma-S_\delta$ atom group on the X-band EPR time scale (*6*). X-ray crystal structures of R1 at helix surface sites in T4L support this conclusion (R. Langen, K.-J. Oh, D. Cascio, H. Mchaourab, and W. L. Hubbell, unpublished data). In this model, the motion of R1 at helix surface sites is limited to rotation about the two terminal bonds nearest the ring (Figure 1), and nearest-neighbor side chain interactions would be minimal because the nitroxide is constrained to move in a limited volume.

In this simple picture, the motion of the R1 side chain is expected to be similar at all exposed helix surface sites, perhaps being enhanced by backbone fluctuations that differ from site to site. In the absence of other interactions, immobilization of the nitroxide is expected to arise only from tertiary steric constraints that modulate bond rotations in the side chain. For the majority of sites investigated in T4L, this is the case. For example, R1 side chains buried in the protein core are strongly immobilized, while those at solvent-exposed tertiary contact sites have multicomponent spectra, one of which reflects some degree of immobilization. Thus, in the context of this model, mobility alone is sufficient to distinguish helix surface sites, tertiary contact sites, and buried sites (*6*).

However, apparent ambiguities arise in particular cases. For example, the EPR spectra of R1 at some fully solvent exposed helix surface sites have two components, one corresponding to a relatively immobilized state. These spectra are essentially degenerate with those at tertiary contact sites (*6*). The origin of the immobilized component is unknown, but it presumably arises from attractive interactions of the nitroxide ring with nearby groups. The presence of such interactions makes it difficult to distinguish tertiary contact sites from helix surface sites on the basis of side chain mobility alone. Moreover, the interpretation of changes in R1 mobility in terms of changes in protein structure may be ambiguous. One approach to solving this problem is through the use of novel nitroxide side chains that limit local attractive interactions.

In the present communication, the nitroxide side chains designated R3, R4, and R5 (Figure 1) are examined on helix surface sites, and R4 and R5 are also examined at tertiary

contact and buried sites. The thioether-linked R3 side chain was previously investigated, and it was found that the nitroxide in R3 has a higher mobility than that in R1 at the same helix surface sites, even though R3 has fewer bonds linking it to the backbone. This is presumably due to the lack of the disulfide bond−main chain interaction (*6*). Here we show that R3 apparently interacts with the nearest-neighbor $i+4$ residue on the surfaces of helices at sites where R1 shows no similar interaction. Thus R3 mobility depends on primary structure of the protein.

The alkylmercury-linked side chain R4 has approximately the same length as R1 and essentially the same volume, but has a different geometry due to the linearity of the S−Hg−C bond. It is shown here that the nitroxide in R4 does not experience immobilizing interactions to the same degree as R1 at helix surface sites and is more suitable for unambiguous identification of tertiary contact interactions.

The R5 side chain is a saturated analogue of R1 and is expected to have the same configuration of the $C_\alpha-C_\beta-S_\gamma-S_\delta$ atom group. Nevertheless, the nitroxide in R5 shows significantly higher mobility and reduced interactions with the protein at helix surface sites, compared with R1, and, like R4, is useful in distinguishing helix surface from tertiary contact sites.

EXPERIMENTAL PROCEDURES

*Synthesis of Spin Labels **I** and **III***. The spin label reagents **I** and **III** were prepared as previously described (*39*, *40*).

*Synthesis of Spin Label **IV***. To a stirred solution of the 3-(bromomethyl)-2,2,5,5-tetramethyl-2,5-dihydro-1*H*-pyrrol-1yloxy radical (*40*) (1.65 g, 5.0 mmol) in dry tetrahydrofuran (40 mL) under N_2 was added NaI (1.50 g, 10.0 mmol), the mixture was stirred for 1 h at room temperature, Hg (2.0 g, 10.0 mmol) was added, and the stirring was continued for another 3 h. The reaction mixture was decanted from the remaining Hg, and the organic phase was washed with water (2×10 mL) and dried over $MgSO_4$. After removal of the solvent, the residue was purified by flash chromatography on silica gel (Kieselgel 60, 0.04−0.06 mm) with hexanes−ethyl acetate to give 950 mg of the 3-(iodomercuriomethyl)-2,2,5,5-tetramethyl-2,5-dihydro-1*H*-pyrrol-1-yloxy radical as a yellow crystalline solid (yield 39%). The melting point was 165−167 °C, and the R_f on TLC (hexane/ethyl acetate, 2:1; Kieselgel 60 F_{254}) was 0.68. The calculated composition (wt %) for $C_9H_{15}HgINO$ is C, 22.49; H, 3.15; and N, 2.91. The analytical composition was C, 22.54; H, 3.04; and N, 2.89.

*Synthesis of Spin Label **V***. To a stirred solution of the 3-(hydroxymethyl)-2,2,5,5-tetramethylpyrrolidin-1-yloxy radical (1.72 g, 10.0 mmol) and triethylamine (1.11 g, 11.0 mmol) in dry CH_2Cl_2 (30 mL) was added methanesulfonyl chloride (1.26 g, 11.0 mmol) dropwise at −78 °C. The mixture was then allowed to warm to room temperature and stirred for another 1 h. The organic phase was washed with brine, dried over $MgSO_4$, and evaporated. The residue was taken up in dry acetone, and NaI (2.25 g, 15 mmol) was added. The mixture was stirred and refluxed for 24 h. The acetone was evaporated, and the residue was taken up in brine (40 mL), extracted with diethyl ether (3×15 mL), and dried over $MgSO_4$. The organic solvent was evaporated, and the oily residue was purified by silica gel chromatography (Kieselgel 60, 0.0400.06 mm), eluting with hexane−diethyl ether, to give the 3-(iodomethyl)-2,2,5,5-tetramethylpyrrolidin-1-yloxy radical as yellow crystals (1.27 g, 45% yield). This compound (846 mg, 3.0 mmol) and $NaSSO_2-CH_3$ (800 mg, 6.0 mmol) were dissolved in dimethyl sulfoxide (DMSO) (10 mL) and heated cautiously at 70 °C for 30 min. The DMSO was evaporated, water was added (30 mL), the mixture was extracted with $CHCl_3$ (3×20 mL), and the organic phase was dried with $MgSO_4$. The solvent was then evaporated, and the residue was purified by silica gel chromatography (Kieselgel 60, 0.04−0.06 mm), eluting with hexanes−ethyl acetate, to give the 3-(methanesulfonylthiomethyl)-2,2,5,5-tetramethylpyrrolidin-1-yloxy radical as a brown solid (240 mg, 30% yield). The melting point was 85−87° C, and the R_f on TLC (hexane/ethyl acetate, 2:1; Kieselgel 60 F_{254}) was 0.24. The calculated composition (wt %) for $C_{10}H_{20}NO_3S_2$ is C, 45.09; H, 7.57; N, 5.26; and S, 24.07. The analytical composition was C, 44.89; H, 7.55; N, 5.27; and S, 24.21.

Preparation of Cysteine Substitution Mutants, Spin Labeling, and EPR Spectroscopy. Mutants of T4L will be designated by giving the single letter code for the original residue, the sequence number, and the single letter code for the new residue. For example, in the T4L mutant D72C, the native Asp residue at position 72 is replaced with Cys.

The mutants D72C, D72C/R76A, D72C/R76A/Q69A/N68A, V131C, V131C/K135A, D61C, and T109C, all prepared in a cysteine-less psuedo-wild-type background, were previously reported (*6*). Single cysteine substitution mutants D72C/Q69A, D72C/N68A, R119C, and R119C/Q123A were prepared and purified in the same cysteine-less background according to previously described procedures (*6*).

In all cases, the modification of T4L mutants with the spin-label reagents was carried out in 20 mM MOPS and 100 mM NaCl, pH 7.2. For labeling with **I** or **V**, the mutants were typically incubated with a 10-fold molar excess of the reagent. The reaction was allowed to proceed at room temperature for at least 4 h for solvent-accessible sites and overnight for buried sites. Labeling of T4L mutants with **III** was carried out in the presence of a 10-fold molar excess of reagent for 12 h at room temperature. For labeling with reagent **IV** the mutants were incubated with a 5-fold molar excess of the reagent at room temperature for 2 h. In each case, excess reagent was removed using a Hi-trap desalting column (Pharmacia Amersham) and concentrated as necessary by centrifugal filtration using Centricon 10 concentrators (Millipore). EPR spectra of all spin-labeled mutants were recorded at X-band in 30% w/w sucrose solution in 20 mM MOPS and 100 mM NaCl, pH 7.2, at ambient temperature in quartz capillaries as previously described (*6*).

RESULTS

Motion of R1, R3, R4, and R5 at Helix Surface Sites and Effects of Nearest-Neighbor Side Chain Substitutions. Helix surface sites are those for which the side chains have a fractional solvent accessibility approaching unity. Figure 2 shows the crystal structure of T4L and the locations of the helix surface sites investigated in this study (D72, R119, V131). The N-terminal helix surface sites 61 and 109 will be discussed separately below.

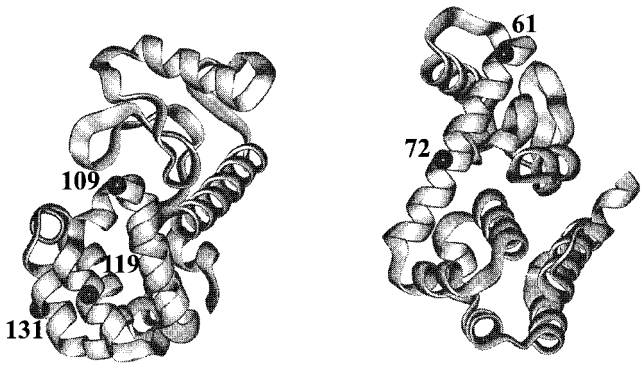

FIGURE 2: Structure of T4 lysozyme showing the locations of solvent-exposed helix surface sites selected for introduction of nitroxide side chains.

Site 72, in the middle of the long interdomain helix, was selected for systematic replacement of the nearest-neighbor residues by alanine to evaluate the extent of side chain interactions. Substitution of the native Asp residue at 72 by R1 has little effect on the thermal stability or enzymatic activity of the protein (*6*). In investigating the interaction of spin labels with the nearest-neighbor residues, the $i+3$ site (V75) was not mutated, because it is located at a tertiary contact site that may result in structural changes of the protein (*41*). The $i-3$ and $i\pm4$ neighbors are solvent exposed, making no obvious tertiary contacts in the structure.

Arginine 119 is not an important structural residue (*42*), making it a suitable host site for introduction of spin-labeled side chains. This site was selected here to illustrate the existence of an immobilized state of R1 at a helix surface site.

Matthews and co-workers have carried out extensive mutagenesis at site V131 (*43*). In general, substitutions at this site have little effect on the protein stability, reflecting only the individual amino acid helix propensities. The bulky $i+4$ Lys residue at 135 can project downward toward V131 and might be expected to interact directly with spin-labeled side chains at this site. Thus, an Ala substitution at 135 was examined for effects on the mobility of the side chains at 131.

A qualitative analysis of mobility and the influence of nearest-neighbor substitutions are presented below for each of the nitroxide side chains.

(A) R1 Side Chain. The data in Figure 3a extend the previous study of nearest-neighbor side chain substitutions around 72R1 to include new single Ala substitutions at site N68 or Q69. The EPR spectra for D72R1 and D72R1/R76A were previously reported (*6*) and are included in Figure 3a for comparison. The spectrum of 72R1 with wild-type nearest neighbors is characteristic of a single population of nitroxides undergoing simple anisotropic motion (*44*). As shown in the figure, a single Ala substitution for N68 ($i-4$), Q69 ($i-3$), or the bulky R76 ($i+4$) has little effect on the EPR spectrum and hence on the motion of the nitroxide.

An unusual result is found for the R1 side chain at 119 (Figure 4a). With wild-type nearest-neighbor residues, the 119R1 spectrum reflects two populations of nitroxide, one of which is relatively immobilized (arrow). Moreover, substitution of an Ala residue for Q123 at $i+4$ produces an increase in the population of the more immobilized state. This behavior illustrates the potential complexity of interaction of the R1 side chain with the protein at specific sites.

The spectrum of R1 at site 131, like that at 72, reflects a dominant population of spin undergoing anisotropic motion. However, 131R1 has a higher mobility, as reflected in the smaller separation of the hyperfine extrema (*44*) and narrower central line width (Figure 5a). Substitution of the $i+4$ Lys residue by Ala results in only subtle changes in the spectrum, retaining the essential features of the anisotropic line shape.

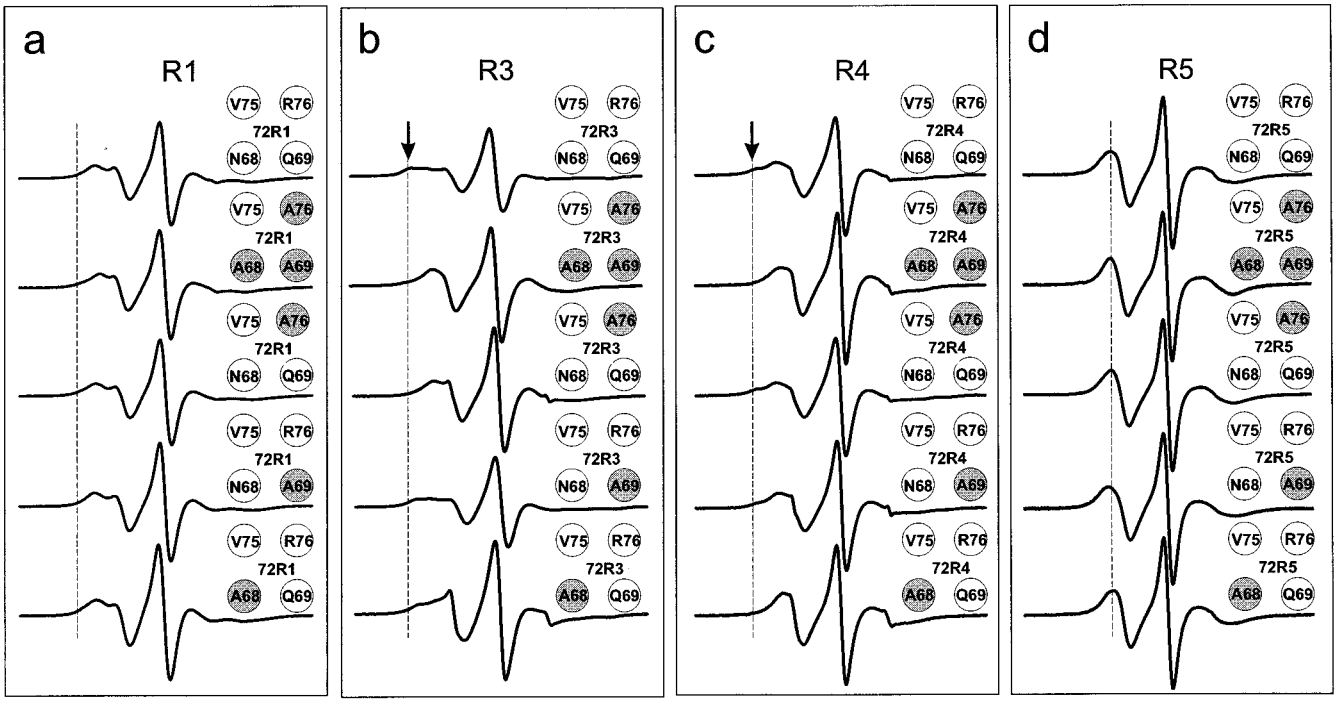

FIGURE 3: EPR spectra of the nitroxide side chains at site 72 with wild-type nearest neighbors (top spectrum) and with the indicated substitutions by alanine (shaded circles): (a) R1; (b) R3; (c) R4; (d) R5.

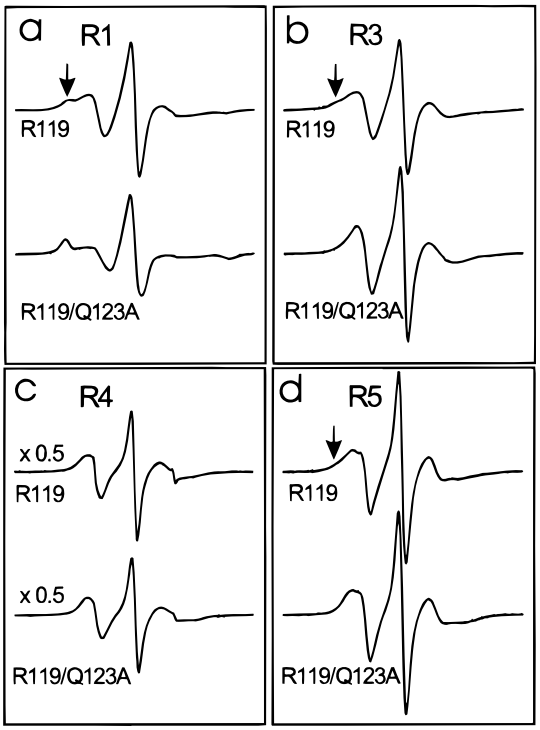

FIGURE 4: EPR spectra of the nitroxide side chains at site 119 with wild-type nearest neighbors (top spectrum) and with the $i+4$ glutamine substituted by alanine (bottom spectrum): (a) R1; (b) R3; (c) R4; (d) R5.

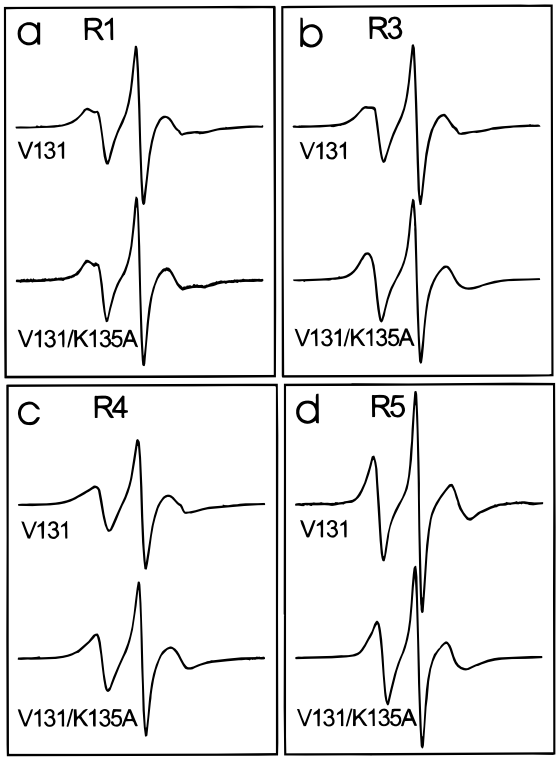

FIGURE 5: EPR spectra of the nitroxide side chains at site 131 with wild-type nearest neighbors (top spectrum) and with the $i+4$ lysine substituted by alanine (bottom spectrum): (a) R1; (b) R3; (c) R4; (d) R5.

(B) R3 Side Chain. The R3 side chain is linked to the backbone by a thioether bond rather than by a disulfide as in R1 (Figure 1). Figure 3b shows the spectra of 72R3 with the same nearest-neighbor substitutions as for 72R1. With the wild-type residues at the nearest-neighbor sites, R3 has a complex multicomponent spectrum, one of which corresponds to a strongly immobilized state (arrow). As can be seen, the single Ala replacement for the bulky $i+4$ Arg at 76 dramatically reduces the immobilized component, suggesting a direct interaction with the $i+4$ side chain.

A similar effect is noted for substitutions at the $i+4$ position around R3 at sites 119 and 131 (Figures 4b and 5b). At 119, R3 again has a multicomponent spectrum, the less mobile component of which is eliminated by the substitution of Ala for Gln 123 at $i+4$. At 131, the R3 spectrum can be described by a single population of nitroxide undergoing anisotropic rotation similar to 72R1, but with a higher mobility. Substitution of the $i+4$ Lys residue by Ala apparently removes a constraint on that motion as evidenced by the essentially isotropic motion in the spectrum of 131R3/K135A.

Substitution at the $i-3$ position has little effect on the spectrum of R3 at position 72 (Figure 3b). However, substitution for Ala at N68 ($i-4$) leads to an increase in the mobility of the more immobilized component of R3 at site 72, suggesting that both $i+4$ and $i-4$ interactions are significant.

(C) R4 Side Chain. The reaction of the alkylmercury reagent **III** with sulfhydryl groups generates the spin-labeled side chain designated as R4. Figure 3c shows the spectra of 72R4, again with the same nearest neighbor substitutions as for 72R1. For 72R4 with wild-type nearest-neighbors, the spectrum reveals two populations of nitroxides with different motional states, one being relatively immobilized (arrow). Substitution of the $i+4$ Arg or the $i-3$ Gln with Ala has essentially no effect on the spectrum. Substitution at the $i-4$ Asn results in a loss of the immobilized component.

At site 119, R4 has a significantly higher mobility than that for R1 at the same site, with no evidence of multiple populations (except for a minor amount of free nitroxide in solution; Figure 4c). Similarly, the spectrum of R4 at 131 is characteristic of a single population, although the "tail" in the low-field resonance line may arise from rapid exchange between multiple states (Figure 5c). At both sites, substitution of the $i+4$ residue by Ala results in little change in the R4 spectra.

(D) R5 Side Chain. The EPR spectrum of R5 at site 72 with wild-type nearest-neighbor side chains apparently consists of a single component with significantly sharper features than that for R1 at the same site (Figure 3d). The sharper features imply that the motion of R5 more effectively averages the anisotropy in the nitroxide hyperfine and *g*-factor tensors compared to R1. Nearest-neighbor side chain substitutions by Ala have little effect at any position.

The spectrum of 119R5 with wild-type nearest neighbors, like 119R1, is apparently multicomponent. However, in this case the more immobile component is reduced relative to R1, showing up only as a shoulder on the low-field resonance line (arrow). Unlike the situation for R1, replacement of the $i+4$ Gln by Ala results only in a modest change in line shape, with a decrease in the population of the more immobile component.

The spectrum of 131R5 is very sharp, indicating effective isotropic motion of the nitroxide with little effect of substitution of the $i+4$ Lys by Ala.

Table 1: Effects of Nearest-Neighbor Substitutions on Side Chain Motion[a]

mutant	R1	R3	R4	R5
72/R76A (*i*+4)	0	++	0	0
72/Q69A (*i*−3)	0	0	0	0
72/N68A (*i*−4)	0	+	+	0
119/Q123A (*i*+4)	−	+	0	+
131/K135A (*i*+4)	0	+	0	0

[a] Each entry gives the effect of the listed Ala substitution on the mobility of the side chain at the indicated site: (+) an increase; (++) a large increase; (−) a decrease.

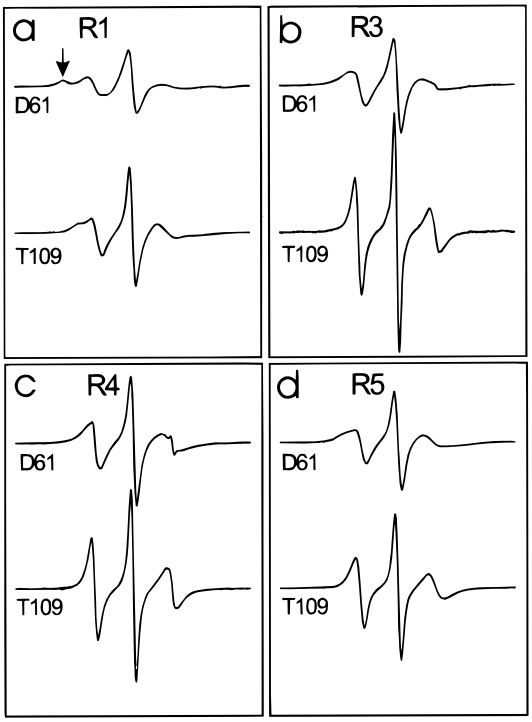

FIGURE 6: EPR spectra of the nitroxide side chains at sites 61 and 109: (a) R1; (b) R3; (c) R4; (d) R5.

A qualitative summary of the effects of nearest-neighbor substitutions by Ala on mobility is provided in Table 1.

N-Terminal Sites. N-Terminal sites are those located in the first turn of an α-helix. R1 residues located at N-terminal helix surface sites have characteristic spectra indicative of two motional states of the nitroxide, distinguishing them from R1 residues at the C-terminal end of the helix and from most interior sites (*6*). Figure 2 shows the location of two N-terminal sites, 61 and 109, and Figure 6 shows the corresponding EPR spectra for the nitroxide side chains at those sites. The spectra of R1 at these sites were previously reported (*6*) and are included for comparison.

At site 61, the spectrum of R1 is clearly resolved to reveal a highly immobilized (arrow) and a mobile population (Figure 6a). At 109, two motional states are also resolved for R1, but with a smaller difference in mobility. The structural origin of the two states is unknown, but it was found that replacement of the N-cap residue with one incapable of capping the helix resulted in disappearance of the more immobilized component. This effect was attributed to dynamic "fraying" of the helix terminus with concomitant increase in motional freedom of the R1 side chain (*6*).

As shown in Figure 6b,c, the R3 and R4 side chains completely lack the interactions necessary to produce the more immobile population and yield spectra characteristic of rapid isotropic motion. The spectrum of the R5 side chain marginally resolves two states at 61, but not at 109.

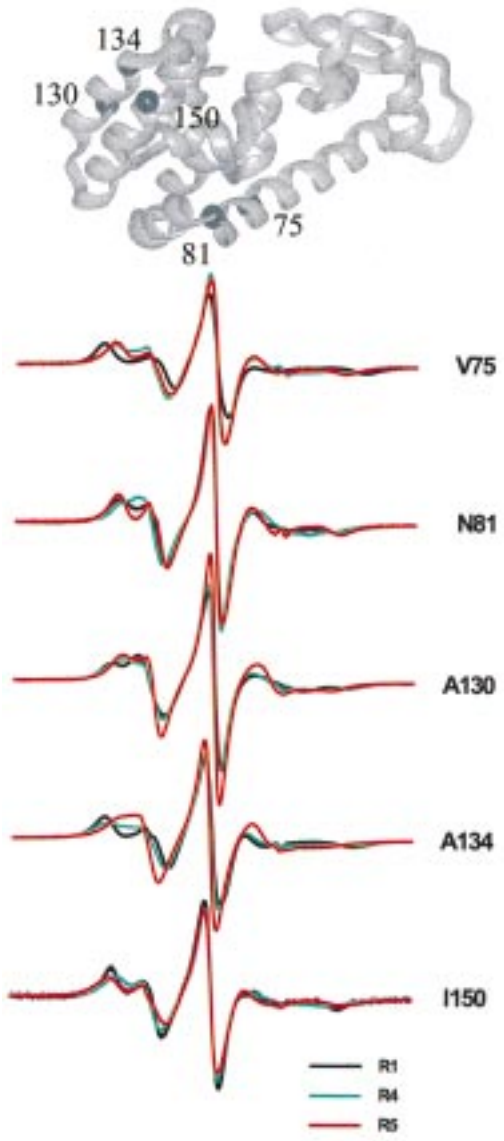

FIGURE 7: (a, top) Structure of T4 lysozyme showing the location of the tertiary contact sites investigated. (b, bottom) Superposition of the EPR spectra for the R1, R4, and R5 side chains at each position.

Tertiary Contact Sites. Tertiary contact sites are defined as sites at which the nitroxide side chain has unavoidable interactions with residues other than those immediately adjacent in the primary sequence. Such interactions constrain the motion of the nitroxide, distinguishing them from helix surface sites (*6*). Locations of the tertiary contact sites 75, 81, 130, 134, and 150 and the corresponding EPR spectra for R1, R4, and R5 are shown in Figure 7. These sites are located at helix−helix contact faces and have fractional solvent accessibilities, calculated by the method of Lee and Richards (*45*), in the range of 0.1−0.3. The reactivity of the alkyl iodide reagent **III** is low at such sterically constrained sites, and it was not possible to examine the properties of the R3 side chain. The R1, R4, and R5 side chains all have spectra indicating a reduced mobility relative to typical exposed helix surface sites, some having multiple components. However, the line shapes of R1 at contact sites 81

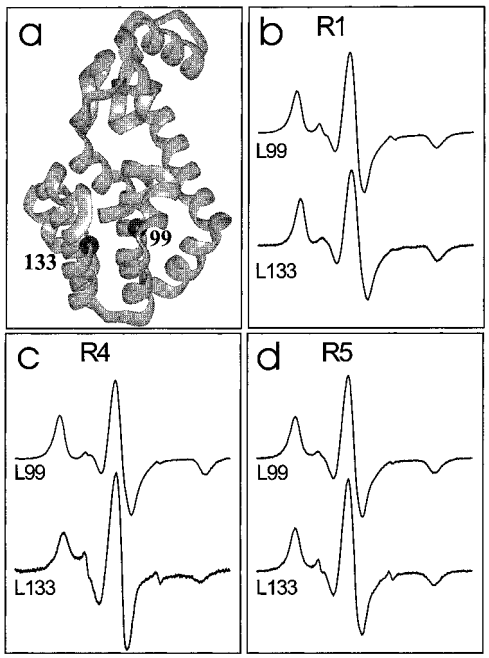

FIGURE 8: (a) Structure of T4 lysozyme showing the location of buried sites 99 and 133. (b−d) EPR spectra of R1, R4, and R5 at sites 99 (top spectrum) and 133 (bottom spectrum).

and 130 are not clearly distinguishable from some of the helix surface sites. For example, the spectra of R1 at sites 72 (Figure 3a) and 81 are similar, as are the spectra of R1 at 119 (Figure 4a) and 130. On the other hand, the spectra of R5 are uniquely immobilized at each contact site compared to helix surface sites.

Thus for unambiguous identification of contact sites in a structure based solely on nitroxide side chain mobility, R5 is apparently the most suitable and removes the spectral degeneracy between contact and exposed sites previously noted. Only at surface site 72 does R4 show any sign of immobilization of the nitroxide ring. Thus, it also provides a useful tool for resolving these sites.

Buried Sites. Buried sites are defined as solvent-inaccessible sites within the core of the protein fold. Figure 8a shows the location and spectra for two such sites, 99 and 133. As expected, R1, R4, and R5 at these sites have spectra corresponding to an immobilized nitroxide (Figure 8b−d). Again, the alkyl iodide reagent **III** shows poor reactivity at these sites due to steric constraints and was not studied.

Secondary Structure Determination. Side chain mobility provides specific information on both tertiary and secondary structural features of a protein. For example, the periodic variation of R1 side chain mobility with sequence position has been found to identify α-helical structures and β-structures (*2*). As shown above, the R5 side chain shows the highest apparent mobility at most solvent-exposed sites investigated, although it has the same immobilized state as R1 and R4 at buried sites. Thus the R5 side chain has the largest dynamic range in mobility. This is illustrated in Figure 9 for a nitroxide scan through the short helix 128−135 in T4 L. Here the mobility, estimated by the central line width measure (*6*), is plotted versus sequence position for the R1, R4, and R5 side chains. Clearly, the contrast between buried and exposed sites is greatest for R5, making this side chain the choice for secondary structure determination.

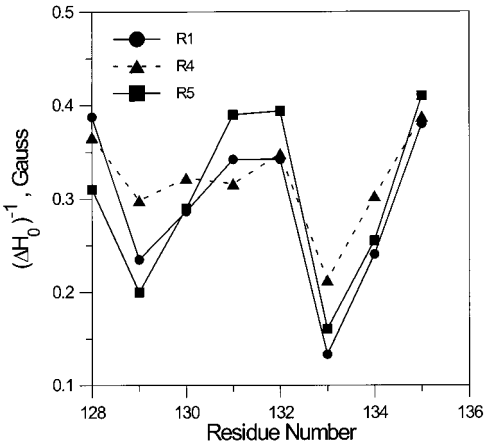

FIGURE 9: Mobility of the nitroxide side chains R1, R4, and R5, measured by the inverse central line width, $(\Delta H_0)^{-1}$, as a function of sequence position through the 2-turn helix 128−135 in T4 lysozyme: (●) R1; (▲) R4; (■) R5.

DISCUSSION

The results presented above represent the first study of the influence of nitroxide side chain structure on mobility in helical proteins. The quantitative analyses of the spectra of R1, R3, R4, and R5 in terms of detailed motional models at particular sites will be the subject of future studies. However, qualitative considerations will serve to understand the salient features of the spectra for the various side chains in the simplest case, that is, for the side chains at noninteracting helix surface sites.

As indicated in Figure 1, the dominant motions of R1 at helix surface sites are rotations about the $S_\delta-C_\epsilon$ and $C_\epsilon-C_\zeta$ bonds of the side chain, due to the stabilizing interaction of the disulfide with the mainchain, as discussed above. Molecular models indicate that rotation about the $S_\delta-C_\epsilon$ bond is relatively unrestricted. Because this axis of rotation is approximately parallel to the nitroxide *z* molecular axis ($2p\pi$ orbital axis) in the minimum energy conformation, rotation about this bond only averages the small $x-y$ anisotropy of the nitroxide **A** (hyperfine) and **g** tensors. Rotation about the $C_\epsilon-C_\zeta$ bond, approximately perpendicular to the nitroxide *z* axis, produces "wobbling" of the $2p\pi$ orbital and averages the large $z-x$ and $z-y$ anisotropies in **A** and **g**. However, rotation about $C_\epsilon-C_\zeta$ is constrained due to the steric interaction of the bulky nitroxide α-methyl substituent and the ring 4-H atom with the sulfurs of the disulfide. Thus the overall motion is a large amplitude oscillation about the *z*-axis with a constrained wobble of the *z*-axis itself. Anisotropic motion of this type has been previously analyzed for the nitroxide, and the general features of the spectral line shapes of R1 at sites 72 and 131 are consistent with this motion (Figures 3a and 5a) (*44*). Within the context of this model, the angular amplitude of wobble of the $2p\pi$ orbital in 131 is greater than at 72, as indicated by the smaller separation of the outer hyperfine extrema in the former, perhaps reflecting additional motional contributions from backbone fluctuations. The lack of interaction of R1 with nearest-neighbor side chains on the helix surface (Figures 3a and 5a) is rationalized by this model, because the dominant bond rotations constrain the motion of the nitroxide to a localized volume which does not significantly overlap the preferred conformational space of the nearest neighbors.

In R5, the saturated analogue of R1, rotations about the $S_\delta-C_\epsilon$ and $C_\epsilon-C_\zeta$ bonds are relatively unrestricted and restricted, respectively, as in R1. However, due to the sp^3 geometry of the 3-carbon in the saturated ring of R5, the axis of the $S_\delta-C_\epsilon$ bond is now approximately perpendicular to the molecular *z*-axis of the nitroxide. Thus, unlike the situation in R1, motion about the $S_\delta-C_\epsilon$ bond effectively averages the largest magnetic anisotropies giving rise to much sharper spectral features for R5 relative to R1 at the same sites. This situation emphasizes that care must be exercised in relating line shapes to mobility when comparing different side chains. In the case of R1 and R5, both nitroxides are likely to have similar mobility, but the spectra are very different due to the different bonding structure in the side chains. The motional model again rationalizes the lack of nearest-neighbor side chain interaction with R5 (Figures 3d and 5d).

Whether the S−Hg group in R4 interacts with main chain atoms in a fashion similar to that of the S−S of R1 is unknown. However, in R4, there is relatively free rotation about the bonds in the linear group $S_\gamma-Hg_\delta-C_\epsilon$, both of which are roughly perpendicular to the nitroxide molecular *z*-axis. Thus this rotation produces effective averaging of the main magnetic anisotropies, consistent with the relatively sharp spectral features of R4 at all sites except 72 (see below).

Side chain R3 has relatively unrestricted rotation about the $C_\beta-S_\gamma$ bond. Together with rotations about the more distal bonds adjacent to the nitroxide ring, the overall motion can be of high amplitude, effectively averaging the nitroxide magnetic anisotropies and giving rise to rather sharp spectral line shapes at sites where specific ring interactions do not occur (Figures 3b, 4b, and 5b). However, the motions allow the ring to explore a large volume of conformational space, making the probability of local interactions significant (see below).

The above considerations generally account for the spectra of the various side chains at exposed helical sites. However, there are interesting exceptions. For example, the spectrum of R1 at the fully exposed helix surface site 119 does not correspond to the expected simple motion described above. Rather, it has multiple components, one of which corresponds to a relatively immobile nitroxide on the EPR time scale (Figure 4a). Moreover, the fraction of the immobile component increases in the mutant 119R1/Q123A. Likewise, the spectra of R1 at the N-terminal helix surface sites 61 and 109 are also multicomponent (Figure 6a). The specific origin of the immobile components in these spectra is uncertain, although it is likely due to attractive interactions of the nitroxide ring with its environment. The interaction could be due to the hydrophobic nature of the nitroxide ring, the hydrogenbond forming capacity of the nitroxide itself, or electrostatic interactions involving the nitroxide dipole moment.

The immobilized component observed for R1 at 119, 61, and 109 is dramatically reduced or absent in the spectra of R4 or R5 at those same sites (Figures 4c,d and 6c,d), and the spectra are now consistent with expectations for these side chains at noninteracting helix surface sites, as can be seen by comparison of the various spectra in Figures 3−6. This result is of practical importance for structure determination by SDSL, because R4 and R5 unambiguously identify 119, 61, and 109 in T4L as exposed helix surface sites, in agreement with the high fractional solvent accessibility computed from crystal structure. On the other hand, the spectra of R1 at these sites are degenerate with those at tertiary contact sites, leading to ambiguity in structural assignment based on mobility alone.

At present, the reason for the apparent reduction in interaction of R4 and R5 with the protein compared to R1 is as uncertain as the nature of the interaction itself, and an explanation must await structure determination of the labeled proteins. However, the difference in behavior is undoubtedly related to the different geometry of each of the side chains. In the simplest view, the linear S−Hg−C group in R4 and the sp^3 ring carbon in R5 could result in conformations that limit the ability of the ring to make maximal contact interactions.

While R4, like R5, exhibits simple spectra at most helix surface sites, 72R4 is a notable exception (Figure 3c) with an EPR spectrum exhibiting a strongly immobilized component. The interaction giving rise to the immobilized state is apparently with N68 at the $i-4$ position, because mutation of that site to Ala eliminates the immobilized component (Figure 3c). The mutation N68A does not in itself change the structure of the protein around 72, because the spectra of 72R1 and 72R1/N68A are similar. Modeling of the R4 side chain in a helix indicates that a direct interaction of the ring with N68 is possible due to the geometry of the R4 side chain, and at the present time this is the favored interpretation of the data.

While R1, R4, and R5 generally show weak or absent nearest-neighbor interactions, at helix surface sites (with the exception noted above), R3 shows a consistent increase in mobility upon replacement of the $i+4$ residue by Ala at the three sites investigated (72R3/K76A, 119R3/Q123A, 131R3/K135A). The lack of effect of the same Ala substitutions for R1, R4, or R5 at these sites indicates that no structural change in the protein is produced by the $i+4$ substitution. In addition, no effect is produced in the motional state of R3 (or any of the side chains) by substitution of Ala for the $i-3$ residue. These results are in accord with models of the R3 side chain on a helical surface. Cysteine occupies one of two rotomeric states about the $C_\alpha-C_\beta$ bond, $X_1 = -180$ and -60, and the R3 state probably has similar conformations. In the $X_1 = -180$ state, the nitroxide would be in direct contact with the $i+4$ residue, but in neither value of X_1 can the nitroxide contact the $i-3$ residue.

Collectively, the data presented in this paper indicate that, of the residues examined, R5 has the least propensity for interaction with nearby structures in the protein. As a result, its mobility is primarily determined by tertiary contact interactions, and R5 is the clear choice for experiments designed to mdap topography and secondary structure by nitroxide scanning. This latter application is illustrated in Figure 9. The greater contrast in mobility as measured by inverse line width between buried and helix surface sites afforded by R5 compared to R1 and R4 is due to the more effective averaging of the magnetic anisotropies in R5 at surface sites.

SUMMARY AND CONCLUSIONS

In summary, the results presented here emphasize potential interactions of the unsaturated nitroxide ring in the side chain

R1 that can occur with the protein at particular solvent-exposed helix surface sites. The interaction results in immobilization of the nitroxide ring, which may lead to ambiguity in interpreting protein topography from mobility data. This ambiguity may be resolved by the use of the saturated analogue R5 that appears to lack the complicating interaction, at least at the sites studied. The mercury-linked side chain R4 may prove useful in this regard as well, but this side chain also showed an immobilizing interaction at one of the sites investigated (72).

Due to the bonding geometry in R4 and R5, the spectral line shapes are much sharper compared to those of R1 at surface sites. Thus, the spectral contrast between buried and surface sites is greater for these side chains compared to R1, and they are preferred for determination of secondary structure by nitroxide scanning experiments.

The R3 side chain is of limited use, due to its low reactivity at tertiary contact and buried sites. Nevertheless, it has the advantage of chemical stability conferred by the thioether bond and shows interactions with the $i+4$ nearest-neighbor residues at helix surface sites. Thus it may find use in situations where modulation of nearest-neighbor side chain interactions are of primary interest.

ACKNOWLEDGMENT

The authors thank Linda Columbus and Dr. Christian Altenbach for helpful discussions and reading of the manuscript.

REFERENCES

1. Hubbell, W. L., and Altenbach, C. (1994) *Curr. Opin. Struct. Biol. 4*, 566−573.
2. Hubbell, W. L., Mchaourab, H. S., Altenbach, C., and Lietzow, M. A. (1996) *Structure 4*, 779−783.
3. Hubbell, W. L., Gross, A., Langen, R., and Lietzow, M. A. (1998) *Curr. Opin. Struct. Biol. 8*, 649−656.
4. Altenbach, C., Marti, T., Khorana, H. G., and Hubbell, W. L. (1990) *Science 248*, 1088−1092.
5. Freed, J. H., and Schneider, D. J. (1989) in *Biological Magnetic Resonance, Vol. 8, Spin Labeling Theory and Applications* (Berliner, L. J., and Reuben, J., Eds.) pp 1−76, Plenum Press, New York.
6. Mchaourab, H. S., Lietzow, M. A., Hideg, K., and Hubbell, W. L. (1996) *Biochemistry 35*, 7692−7704.
7. Mchaourab, H. S., Oh, K.-J., Fang, C. J., and Hubbell, W. L. (1997) *Biochemistry 36*, 307−316.
8. Likhtenshtein, G. I. (1976) *Spin Labeling Methods in Molecular Biology*, Wiley-Interscience, New York.
9. Rabenstein, M. D., and Shin, Y.-K. (1995) *Proc. Natl. Acad. Sci. U.S.A. 92*, 8239−8243.
10. Voss, J. C., Salwinski, L., Kaback, H. R., and Hubbell, W. L. (1995) *Proc. Natl. Acad. Sci. U.S.A. 92*, 12295−12299.
11. Hustedt, E. J., Smirnov, A. I., Laub, C. F., Cobb, C. E., and Beth, A. H. (1997) *Biophys. J. 74*, 1861−1877.
12. Steinhoff, H.-J., Radzwill, N., Thevis, W., Lenz, V., Brandenburg, A. A., Dodson, G., and Wollmer, A. (1997) *Biophys. J. 73*, 3287−3298.
13. Altenbach, C., Flitch, S., Marti, T., Khorana, H. G., and Hubbell, W. L. (1989) *Biochemistry 28*, 7806−7812.
14. Greenhalgh, D., Altenbach, C., Hubbell, W. L., and Khorana, H. G. (1991) *Proc. Natl. Acad. Sci. U.S.A. 88*, 8626−8630.
15. Altenbach, C., Greenhalgh, D., Khorana, H. G., and Hubbell, W. L. (1994) *Proc. Natl. Acad. Sci. U.S.A. 91*, 1667−1671.
16. Farahbakhsh, Z., Ridge, K. D., Khorana, H. G., and Hubbell, W. L. (1995) *Biochemistry 34*, 8812−8819.
17. Altenbach, C., Yang, K., Farrens, D. L., Farahbakhsh, Z., Khorana, H. G., and Hubbell, W. L. (1996) *Biochemistry 35*, 12470−12478.
18. Yang, K., Farrens, D. L., Altenbach, C., Hubbell, W. L., and Khorana, H. G. (1996) *Biochemistry 35*, 14040−14046.
19. Farrens, D. L., Altenbach, C., Yang, K., Hubbell, W. L., and Khorana, H. G. (1996) *Science 274*, 768−770.
20. Cai, K., Langen, R., Hubbell, W. L., and Khorana, H. G. (1997) *Proc. Natl. Acad. Sci. U.S.A. 94*, 14267−14272.
21. Kim, J.-M., Altenbach, C., Thurmond, R., Khorana, H. G., and Hubbell, W. L. (1997) *Proc. Natl. Acad. Sci. U.S.A. 94*, 14273−14278.
22. Todd, A. P., Cong, J., Levinthal, F., Levinthal, C. and Hubbell, W. L. (1989) *Proteins: Struct., Funct., Genet. 6*, 294−305.
23. Zhan, H., Oh, K.-J., Shin, Y.-K., Hubbell, W. L., and Collier, R. J. (1995) *Biochemistry 34*, 4856−4863.
24. Oh, K. J., Zhan, H., Cui, C., Hideg, K., Collier, R. J., and Hubbell, W. L. (1996) *Science 273*, 810−812.
25. Berengian, A. R., Bova, M. P., and Mchaourab, H. S. (1997) *Biochemistry 36*, 9951−9957.
26. Mchaourab, H. S., Berengian, A. R., and Koteiche, H. A. (1997) *Biochemistry 36*, 14627−14634.
27. Klug, C. S., Su, W., and Feix, J. B. (1997) *Biochemistry 36*, 13027−13033.
28. Klug, C. S., Eaton, S. S., Eaton, G. R., and Feix, J. B. (1998) *Biochemistry 37*, 9016−9023.
29. Voss, J., Hubbell, W. L., and Kaback, H. R. (1998) *Biochemistry 37*, 211−216.
30. Voss, J., He, M., Hubbell, W. L., and Kaback, H. R. (1996) *Biochemistry 35*, 12915−12918.
31. Langen, R., Issa, J. M., Leucke, H., Haigler, H., and Hubbell, W. L. (1998) *J. Biol. Chem. 273*, 22453−22457.
32. Perozo, E., Cortes, D. M., and Cuello, L. G. (1998) *Nat. Struct. Biol. 5*, 459−469.
33. Farahbakhsh, Z., Hideg, K., and Hubbell, W. L. (1993) *Science 262*, 1416−1420.
34. Steinhoff, H.-J., Mollaaghababa, R., Altenbach, C., Hideg, K., Krebs, M., Khorana, H. G., and Hubbell, W. L. (1994) *Science 266*, 105−107.
35. Thorgeisson, T. E., Xiao, W., Brown, L. S., Needleman, R., Lanyi, J. K., and Shin, Y.-K. (1997) *J. Mol. Biol. 273*, 951−957.
36. Rink, T., Riesle, J., Oesterhelt, D., Gerwert, K., and Steinhoff, H.-J. (1997) *Biophys. J. 73*, 983−993.
37. Shin, Y., Levinthal, C., Levinthal, F., and Hubbell, W. L. (1993) *Science 259*, 960−963.
38. Qu, K., Vaughn, J. L., Sienkiewicz, A., Scholes, C. P., and Fetrow, J. S. (1997) *Biochemistry 36*, 2884−2897.
39. Berliner, L. J., Grunwald, J., Hankovszky, H. O., and Hideg, K. (1982) *Anal. Biochem. 119*, 450−455.
40. Hankovszky, H. O., Hideg, K., and Lex, L. (1980) *Synthesis*, 914−916.
41. Matsumara, M., Becktel, W. J., and Matthews, B. W. (1988) *J. Mol. Biol. 246*, 317−330.
42. Blaber, M., Baase, W. A., Gassner, N., and Matthews, B. W. (1995) *J. Mol. Biol. 246*, 317−330.
43. Zhang, X.-J., Baase, W. A., and Matthews, B. W. (1992) *Protein Sci. 1*, 761−776.
44. Hubbell, W. L., and McConnell, H. M. (1971) *J. Am. Chem. Soc. 93*, 314−326.
45. Lee, B., and Richards, F. M. (1971) *J. Mol. Biol. 200*, 379−400.

BI9826310